Journal of Power Sources 189 (2009) 1093–1099

Contents lists available at ScienceDirect

Journal of Power Sources

journal homepage: www.elsevier.com/locate/jpowsour

High-temperature mechanical properties of a glass sealant for solid oxide fuel cell

Hsiu-Tao Chang[a], Chih-Kuang Lin[a,*], Chien-Kuo Liu[b]

[a] Department of Mechanical Engineering, National Central University, Jhong-Li 32001, Taiwan
[b] Nuclear Fuel & Material Division, Institute of Nuclear Energy Research, Lung-Tan 32546, Taiwan

ARTICLE INFO

Article history:
Received 20 November 2008
Received in revised form
22 December 2008
Accepted 22 December 2008
Available online 31 December 2008

Keywords:
Planar solid oxide fuel cell
Four-point bending test
High temperature
Weibull statistic analysis
Mechanical properties
Glass transition temperature

ABSTRACT

The high-temperature mechanical properties of a newly developed silicate-based glass sealant, designated as GC-9, have been studied for use in planar solid oxide fuel cell (pSOFC). Four-point bending tests were conducted at room temperature, 550 °C, 600 °C, 650 °C, 700 °C and 750 °C to investigate the variation of flexural strength, elastic modulus, and stress relaxation with temperature for the given glass sealant. Weibull statistic analysis was applied to describe the fracture strength data. The results indicated that the flexural strength was increased with temperature when the testing temperature was below the glass transition temperature (T_g, 668 °C). This was presumably caused by a crack healing effect taking place at high temperatures for glasses. However, with a further increase of temperature to a level higher than T_g, significant stress relaxation was observed to cause extremely large deformation without breaking the specimen. When the controlled displacement rate was increased by an order of magnitude, the stress relaxation effect at 750 °C became less effective. However, the mechanical stiffness of the given glass was significantly reduced at a temperature higher than T_g.

1. Introduction

Planar solid oxide fuel cell (pSOFC) is a high temperature (600–1000 °C) device to convert chemical energy to electricity. Sealant is a critical material in a pSOFC to maintain its operation and performance. It is needed to join components and form gas-tight seals to separate both the oxidant and fuel chambers. Sealants in pSOFC must provide necessary adherence, mechanical integrity, chemical stability and compatibility, electric insulation, and thermal expansion match during operation [1–4]. These requirements create a major challenge in development of a suitable sealant for use in pSOFC. During the fabrication and operation stages, thermal, chemical and mechanical properties of sealants might be changed leading to degradation in performance of a pSOFC. The influence of such properties of sealant cannot be ignored in design of a pSOFC stack. Areas of application of sealant in a pSOFC stack include: (a) cell to metal frame, (b) metal frame to metal interconnect, (c) frame/interconnect to spacer (for electric insulation), and (d) stack to base manifold plate [5]. A sealant should be selected in accordance with operation temperature, application location, and stack design and be compatible with other components. Different sealing designs have been proposed, such as rigid sealing, compressive sealing, and compliant sealing [5,6]. Up to now, glass and glass ceramic materials are the primary candidates in the type of rigid sealing for use in pSOFC stack. Their thermal [1–4,6–18], chemical [4,7,9–21], and mechanical properties [4,14,15] have been investigated for applications in pSOFC. They even could act as compliant seals if an appropriate viscosity range at operation temperature is controlled [5]. However, there is no a specific sealant which can offer a great promise for various pSOFC applications with different ranges of operation temperatures and cell designs.

The sealant must offer sufficient viscosity and good wetting behavior to form well adherent bond during joining process, but it should not soften and flow during operation in order to form a gas-tight seal. Therefore, the glass system used as a sealant material in pSOFC must have a glass transition temperature (T_g) below the operating temperature [2,6]. In addition, significant stresses may develop in pSOFC due to mismatch of coefficient of thermal expansion (CTE) between components and temperature gradients during cyclic thermal operation [22–24]. Therefore, T_g and CTE are two of the important factors need to be taken into account for selection of a suitable glass sealant in pSOFC [6]. Many compositions of glass and glass ceramic sealants for pSOFC use have been developed and their thermal and chemical properties have been extensively studied in [1–21]. For example, phosphate, borosilicate, boroaluminosilicate, silicate glasses and glass-ceramics have been developed and evaluated for use in pSOFC [1–21]. There are volatilization and chemical interaction problems in both phosphate and boron-based glass systems [2,4,5,7,8]. Silicate glasses exhibit less interaction with other SOFC components [4,5]. Unfortunately, their CTE is lower than other SOFC components. Among the silicate-based modifiers developed,

* Corresponding author. Tel.: +886 3 426 7340; fax: +886 3 425 4501.
E-mail address: t330014@cc.ncu.edu.tw (C.-K. Lin).

0378-7753/$ – see front matter © 2008 Elsevier B.V. All rights reserved.
doi:10.1016/j.jpowsour.2008.12.102

alkaline-earth modifiers were used to increase the CTE and improve the adhesion ability [4,6].

For those glasses and glass-ceramics developed for use in pSOFC, their characteristics such as glass composition, crystallization tendency, thermal properties, ratio of glass and binder of paste, joining temperature profile, operation condition, and long-term stabilities were widely investigated [1–21,25–27]. However, there are limited studies focused on the mechanical properties of the glass and glass-ceramic sealants in literature [4,14,15]. Even though a commercial glass sealant, G-18, has been investigated and discussed extensively [4,14,15,28–32], there is still lack of a comprehensive study on the high-temperature mechanical properties of such a glass and glass-ceramic sealant used in pSOFC. However, it is necessary to study the high-temperature mechanical properties of the glass and glass-ceramic sealants so as to assess the structural integrity of a pSOFC stack during cyclic operation.

A new glass sealant of the BaO-B_2O_3-Al_2O_3-SiO_2 system for use in intermediate-temperature pSOFC (IT-pSOFC) at 700–750 °C has been recently developed at the Institute of Nuclear Energy Research (INER). This new glass sealant is a kind of silicate-based glass and is one of the promising glasses to be used in IT-pSOFC. The CTE, viscosity, and crystallization of this sealant, and the chemical interaction between this sealant and other pSOFC components (electrolyte, electrode, interconnect, and frame) have been investigated [33–35]. Based on the results in those studies [33–35], this new glass showed good thermal properties and chemical compatibility with other components and is to be used in a prototypical pSOFC stack being developed at the INER. Therefore, it is important to study its high-temperature mechanical properties so as to provide necessary information for design and development of a reliable pSOFC. The mechanical properties of this newly developed glass sealant at various temperatures are studied in the present work. The aim of this study is to investigate the variation of the elastic modulus, mechanical strength, and stress relaxation behavior with temperature for this glass by systematic four-point bending tests.

2. Experimental procedures

2.1. Material and specimens

The glass sealant used in the present work was developed at the INER for use in IT-pSOFC. Its major composition includes BaO, B_2O_3, Al_2O_3, and SiO_2. The sealant, designated as GC-9, was prepared firstly by melting appropriate amounts of reagents in a powder mixture. The powder mixture was melted at 1550 °C for 10 h and subsequently poured into a mold preheated to 650 °C to produce ingots. The glass ingots were then annealed at 650 °C and cooled down to room temperature. The thermal properties, such as T_g, softening temperature (T_s), crystallization temperature (T_c), and CTE, were measured by differential scanning calorimetry (DSC) and a dilatometer at the INER [33–35]. Fig. 1 shows the DSC curve of the GC-9 glass. The thermal expansion data for the GC-9, sintered GC-9, a positive electrode-electrolyte-negative electrode (PEN) assembly, and Crofer 22-APU steel are shown in Fig. 2 [35]. The T_g, T_s, T_{c1}, and T_{c2} of the GC-9 glass are 668 °C, 745 °C, 820 °C, and 864 °C, respectively. The GC-9 glass shows good CTE match with the PEN and Crofer 22-APU steel. Note that Crofer 22-APU is a steel commonly used as an interconnect material in an IT-pSOFC. According to ASTM C1211 [36] for preparing four-point bending specimens, the glass ingots were cut into rectangular bars with dimensions of 3 mm × 4 mm × 45 mm. The four edges in the cross-section of each specimen were beveled to prevent the stress concentration effect of a right-angle corner. Machining direction was along the 45-mm-length longitudinal direction and the tensile surfaces of the specimens were finally polished by 0.3-μm Al_2O_3 powders.

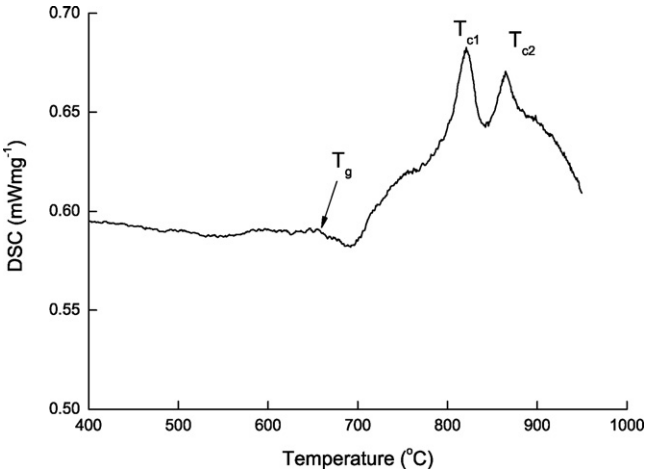

Fig. 1. DSC thermograms for the GC-9 glass.

2.2. Four-point bending test

Four-point bending tests of the GC-9 specimens were conducted as per ASTM C1211 [36] to characterize the mechanical properties of this glass sealant at various temperatures. The four-point bending tests were performed by using a commercial closed-loop servo-hydraulic machine attached with a furnace. The flexural loading fixture with a 20-mm inner loading span and 40-mm outer loading span was made of alumina in order to perform tests at high temperatures. As the T_g, T_s, and expected operating temperature for the GC-9 are 668 °C, 745 °C, and 700–750 °C, respectively, the testing temperatures were set at 25 °C, 550 °C, 600 °C, 650 °C, 700 °C, and 750 °C. For each high-temperature test, the specimen was heated to the specified temperature at a heating rate of 6 °C min^{-1}. The specimen was then held at the specified temperature for 3 min before applying the load. The load was applied under displacement control with a displacement rate of 0.005 mm s^{-1} for all the given testing temperatures. Additional tests at 750 °C were conducted under another displacement rate of 0.05 mm s^{-1} to observe the effects of deformation rate on the high-temperature mechanical properties. The load–displacement relationship was recorded for each test to calculate the flexural strength and other properties. After four-point bending testing, fracture surfaces of broken specimens were

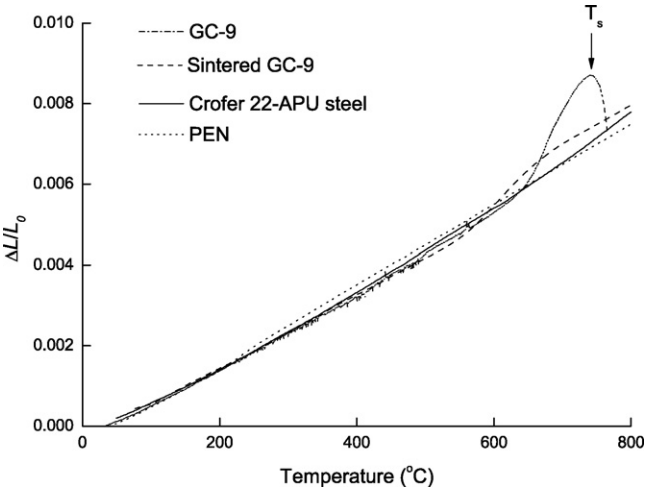

Fig. 2. Thermal expansion curves of GC-9, sintered GC-9, Crofer 22-APU, and PEN [35]. The heat treatment condition for the sintered GC-9 was 850 °C for 1 h followed by 750 °C for 4 h.

observed with scanning electron microscopy (SEM) to identify the fracture origins and mechanisms.

2.3. Weibull statistic analysis

The Weibull statistics [37] is widely applied to describe the fracture behavior of brittle materials. Based on a weakest-link hypothesis, it is assumed that the most severe flaw controls the strength. When subjected to an applied stress, σ, the cumulative probability of failure for a brittle material can be expressed by [37]

$$F = 1 - \exp\left[-\left(\frac{\sigma - \sigma_u}{\sigma_o}\right)^m\right] \quad (1)$$

where F is the failure probability for an applied stress σ, σ_o is a normalizing parameter, σ_u is the threshold stress (below which no failure will occur), and m is the Weibull modulus. Here, the Weibull modulus m is a measure of the degree of strength data dispersion. If σ_u is assumed to be zero, Eq. (1) becomes a two-parameter relation, as shown below [37]

$$F = 1 - \exp\left[-\left(\frac{\sigma}{\sigma_o}\right)^m\right] \quad (2)$$

This two-parameter Weibull probabilistic equation was applied to analyze the scattering and reliability of the strength data generated in the current study. In order to have enough data points for Weibull analysis, seventeen or eighteen specimens were tested at each given testing condition.

2.4. Determination of Young's modulus

According to the flexural theory in mechanics of materials, a linear force–displacement relationship at the inner loading point can be obtained and applied to determine the Young's modulus of the given glass. Thus, the Young's modulus can be determined through the following equation [38]:

$$E = \frac{a^2(4a - 3L)}{6I} \cdot \frac{P}{v} \quad (3)$$

where E is the Young's modulus, I is the moment of inertia for the beam cross-sectional area, v is the vertical displacement at the inner loading point relative to the outer loading point, P is half of the applied force, a is the distance between the inner loading point and the outer loading point on the same side, and L is the outer span length. By applying Eq. (3) to the obtained load–displacement data for each tested specimen, the Young's moduli for the GC-9 glass at various temperatures were determined.

3. Results and discussion

3.1. Influence of environmental temperature on fracture strength

Typical force–displacement curves for the given GC-9 glass under a displacement rate of 0.005 mm s^{-1} at various temperatures are shown in Fig. 3. Arrows in this figure indicate the specimens were not broken when the tests were terminated. The data could be divided into two groups by the testing temperature, i.e., above or below T_g (668 °C) of the GC-9 glass. At temperatures of 25 °C, 550 °C, 600 °C, and 650 °C, the force–displacement curves remained almost linear until final fracture. On the other hand, the force–displacement curves for 700 °C and 750 °C were non-linear and the specimens were deformed considerably without fracture. In fact, T_g of a glass material is the critical temperature at which the material changes its behavior from a glassy state to a supercooled liquid. A glass is defined as a material that has no long-range, periodic atomic and molecular order arrange. Below T_g, large-scale molecular motion is not possible because the material is essentially frozen and it can be treated as a brittle material. Above T_g, molecular motion takes place. Therefore, the fracture behavior of a glass would change from brittle to ductile fracture at a temperature around and above T_g [39].

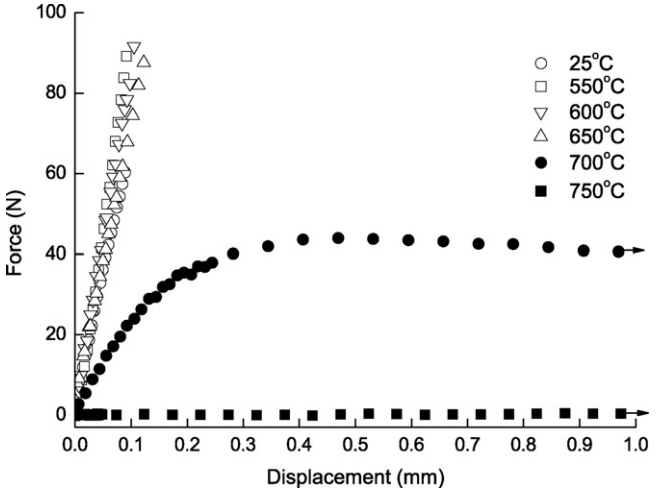

Fig. 3. Typical force–displacement relationship for the GC-9 glass subject to four-point bending under a displacement rate of 0.005 mm s^{-1} at various temperatures.

It is clearly shown in Fig. 3 that the GC-9 glass behaved as a brittle material at a temperature below its T_g (668 °C), and became viscous when the testing temperature was higher than its T_g. Similar trends were also found in four-point bending tests for a commercial G-18 glass from room temperature to 800 °C [15]. The load–displacement curves for G-18 glass were linear until fracture at temperatures up to 700 °C, while the responses were non-linear at temperatures higher than 700 °C [15]. Moreover, another study [4] also found that G-18 failed in a linear elastic manner at room temperature, but exhibited a brittle fracture pattern with non-linear elastic behavior at 750 °C. Since the T_g of G-18 is 630 °C [4], both studies [4,15] showed a similar trend to that of the present work in which the force–displacement relationship was controlled by the T_g of glass. Nguyen et al. [15] indicated that the non-linear response of G-18 glass at high temperature (>700 °C) might be attributed to viscoelastic behavior of porous and glassy phases, void initiation and growth, crystallite/glass phase decohesion, microcracking and/or plasticity of the glassy phases. In the current study, the GC-9 glass was barely crystallized during the short testing period at the given test temperatures. The non-linear response was considered to be caused by viscoelastic and/or plastic flow of the glassy phase when placed at a temperature above T_g of the GC-9 glass. Apparently, viscosity of the GC-9 glass at 700 °C was significantly reduced to enhance the viscoelastic and/or plastic flow so that fracture did not take place when the force reached a maximum value of 47 N. After reaching the peak value of 47 N, the force was continuously relaxed even though a constant displacement rate of 0.005 mm s^{-1} was still applied. Stress relaxation effect obviously became effective at 700 °C under such a displacement rate. At 750 °C, the stress relaxation effect became more pronounced such that the load was almost immediately relaxed to a very small value of 2.5 N with a continuous increase of deformation. Therefore, stress relaxation effect started to play a role in influencing the mechanical performance when the testing temperature was increased to 700 °C. When the testing temperature was further increased to 750 °C, which is greater than the softening temperature (745 °C) of the GC-9 glass, the viscosity dropped to a greater extent so that the specimen could not take too much load for a given deformation rate.

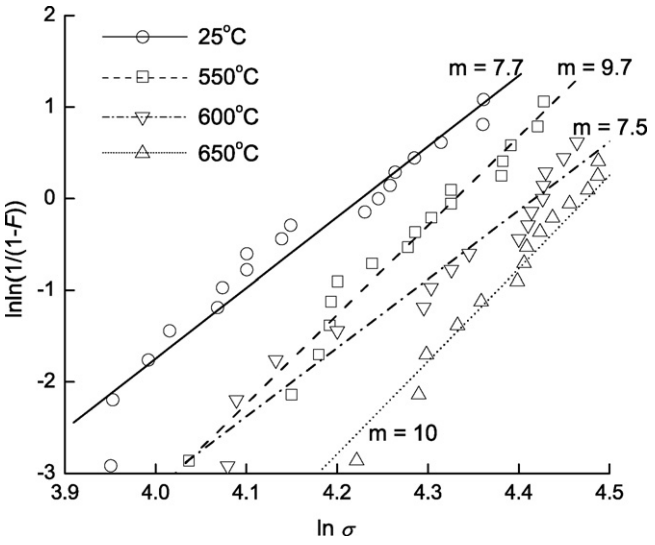

Fig. 4. Two-parameter Weibull distribution of flexural strength for the GC-9 glass.

Fig. 4 shows the two-parameter Weibull distribution of flexural strength for the given GC-9 glass at different temperatures. As shown in Fig. 4, for a given failure probability, the flexural strength was increased with temperature from room temperature to 650 °C. Table 1 lists the mean values of the flexural strength for the given GC-9 glass at various temperatures. Note the data for 700 °C and 750 °C in Table 1 are not the fracture strength but the mean values of the maximum flexural stress applied during test. It is indicated that the flexural strength was increased with temperature from 25 °C to 650 °C. The increase of flexural strength with temperature at temperatures below T_g was presumably attributed to a crack healing effect [40,41]. Such a crack healing effect also caused an improvement in the strength of other glasses [40,42,43]. Because 650 °C is still below T_g of the GC-9 glass, the GC-9 glass behaved as a brittle material. Therefore, the flexural strength of the GC-9 glass is expected to be controlled by the nature and concentration of the flaws present in the specimens. Glass, glass-ceramic and ceramic components or devices tend to have surface defects caused by processing, machining, grinding, thermal shock and/or impact. The crack healing kinetics may take place in glasses and ceramics by annealing at high temperature and is dependent on temperature and aging time. The strength of glasses and ceramics at a certain high temperature can be recovered through this process. The crack healing process in a glass can be divided into four stages: (1) relaxation of residual stress and blunting of crack tip, (2) receding and breaking of crack outlines, (3) rounding and grooving of crack edges, and (4) smoothing and complete healing [40]. When a glass sample is placed in a high-temperature environment, the stress concentration effects of irregularly shaped flaws and cracks might be relaxed due to such a high-temperature healing effect which could cause blunting of crack tips and sharp corners [40,41]. Such a healing effect might take place in the GC-9 bending specimens tested at 550 °C, 600 °C, and 650 °C and change the flaw geometry to a less severe type. At the same time, these three temperatures were below T_g and the testing period was very short so that the viscous effect was not so pronounced. In this regard, the flexural strength of the GC-9 glass was increased with temperature from room temperature to 650 °C.

Table 1
The mean values of flexural strength for GC-9 glass at various temperatures.

Temperature	25 °C	550 °C	600 °C	650 °C	700 °C	750 °C
Flexural strength (MPa)	63	73	82	83	40[a]	4.5[a]

[a] Maximum flexural stress applied during test.

The value of the Weibull modulus, m, was also increased with temperature from room temperature to 650 °C, except 600 °C. In mechanical failure of a brittle material, the Weibull modulus is related to the shape, size, and distribution of strength-controlling flaws. A higher value of m implies a less scattering in strength data and a smaller range of distribution in flaw size and shape. Accordingly, outlines of the surface defects in the GC-9 samples at high temperatures might be different from those at room temperature. Such a difference in the surface defect outline could be attributed to the aforementioned crack healing effect taking place at high temperatures in the GC-9 specimens. Based on a weakest-link hypothesis, the most severe flaw controls the strength of a brittle material. As the crack healing process could relax the stress concentration around surface flaws and change the flaw outlines, the population of the strength-controlling flaws thus became less scattering in the GC-9 specimens tested at high temperatures. In this regard, the m values of 550 °C (m = 9.7) and 650 °C (m = 10) are greater than that at room temperature (m = 7.7). However, the Weibull modulus at 600 °C (m = 7.5) was comparable with that at room temperature. The reason for this exception at 600 °C is not certain at this moment.

When the testing temperature was set greater than T_g, the sharp cracks and surface defects might be healed to a greater extent due to the capillarity-driven viscous flow of glass [40,41,44]. However, a glass starts to flow at a temperature above T_g and brittleness becomes disappearing. It becomes more difficult to activate crack propagation from a preexisting flaw because energy dissipation occurs through viscoelastic and/or plastic flow in the vicinity of the flaw. Eventually, the glass could not be broken and it cannot maintain the mechanical properties as those obtained at lower temperatures. Hence, the maximum applied stress significantly dropped at 700 °C and 750 °C for the GC-9 glass and fracture did not take place at both temperatures. Similarly, Meinhardt et al. [4] showed that for an annealed G-18, which was heat treated for 4 h at 850 °C in ambient air, the flexural strength at room temperature and 750 °C were 85 and 48 MPa, respectively. It is obvious that the viscous flow would relax the high-temperature strength of a glass at a temperature above T_g.

In order to confirm existence of the crack healing effect in the GC-9 glass at high temperatures, a technique of healing Vickers indentations used in [40] was applied in the current study. An annealing treatment was conducted on artificially indented GC-9 specimens to observe the variation of indent outlines. The GC-9 glass samples with one side polished by 0.3-μm alumina powders were indented with a Vickers hardness indenter (9.8 N) and then heat treated at 650 °C for 5 min in air. These GC-9 specimens with Vickers indents were observed with optical microscopy (OM) before and after heat treatment. Outlines of indented subsurface cracks were hardly detectable before heat treatment but became clearly visible after heat treatment, as shown in Fig. 5. Similar phenomenon was also observed in [40]. This change of visibility of subsurface-crack outlines after heat treatment could be attributed to relaxation of the residual stresses induced by indentation [40]. Since the heat treatment time is very short, the Vickers indents on the GC-9 specimens only underwent the first stage of the crack healing process without blunting of the sharp crack tips, as shown in Fig. 5. However, it was enough to change the stress state around a flaw/crack in GC-9 specimens at high temperatures and improve the strength.

3.2. Influence of temperature on Young's modulus

The calculated Young's moduli based on Eq. (3) and measured load–displacement relation at various temperatures are shown in Fig. 6. In this figure, the circle symbol represents the average value

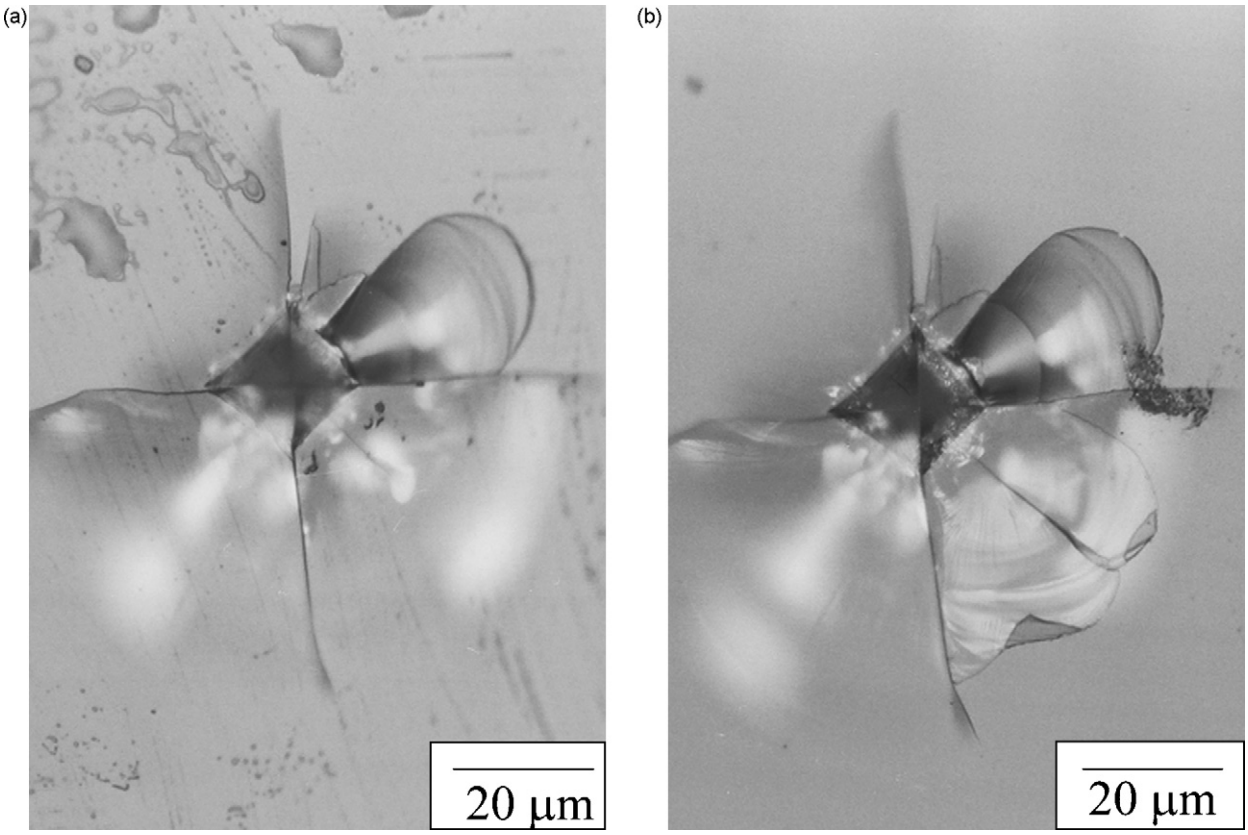

Fig. 5. OM micrographs of a Vickers indent (a) before and (b) after heat treatment. The crack outlines under surface become distinct due to heat treatment.

of the Young's modulus and the ends of the error bar represent the highest and lowest values obtained at a given temperature. Although the Young's modulus data scattered to different extents at all the given temperatures, they may be seen as comparable at room temperature to 600 °C. A slight decrease in the Young's modulus was found at 650 °C, while the Young's modulus value decreased significantly at 700 °C. Apparently, the Young's modulus of the given GC-9 glass was temperature dependent at temperatures around and above T_g. In other words, the GC-9 glass could maintain its stiffness and behaves almost as a brittle material at temperatures blow T_g, as also indicated by the linear force–displacement curves shown in Fig. 3. When a temperature is close to T_g and above, the viscosity of a glass material decreases and a solid state starts to change to a liquid state such that the stiffness decreases with increasing temperature. As the GC-9 glass is expected to be used at 700–750 °C, understanding of its stiffness at such high temperatures is needed. However, its Young's modulus at 750 °C could not be evaluated under a displacement rate of 0.005 mm s^{-1} due to a significant stress relaxation effect. Liu et al. [32] measured the Young's moduli of the G-18 glass at various temperatures by a dynamic resonance technique. The Young's modulus of the G-18 glass was decreased with increasing temperature from 20 °C to 600 °C [32]. However, the dynamic resonance technique cannot determine the Young's modulus of the G-18 at 700 °C and 800 °C [32]. This might have been caused by the softening of the glass phase in the G-18 specimens at such high temperatures [32]. However, from the linear portion of the load–displacement curve obtained by a four-point bending technique, the Young's modulus of the GC-9 glass could be determined at 700 °C in the current study.

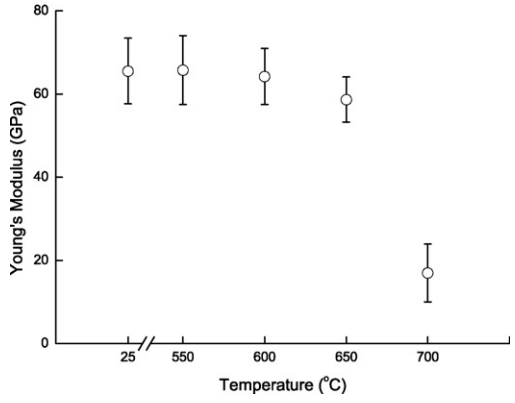

Fig. 6. Young's modulus of the GC-9 glass under a displacement rate of 0.005 mm s^{-1} at different temperatures.

3.3. Fractography analysis

Fracture surface observation with SEM was undertaken for the GC-9 specimens fractured at 25 °C, 550 °C, 600 °C, and 650 °C. Different fracture patterns and morphologies were observed from room temperature to 650 °C, as shown in Fig. 7. These SEM micrographs all show that fracture of each broken specimen was initiated from a chipping zone at a beveled edge on the tensile surface. The surface flaws in this area induced a stress concentration so that the specimens were fractured preferentially at these locations. Apparently, the fracture strength of the GC-9 specimens at a temperature below T_g was controlled by such surface flaws. Although the surface flaws could not be fully healed for a short period of testing time at the given high temperatures, the accompanied stress concentration could be relaxed to different extents and the fracture strength was improved. This might explain why the Young's modulus was barely changed but the flexural strength was increased from room temperature to 600 °C for the given GC-9 glass. The fracture

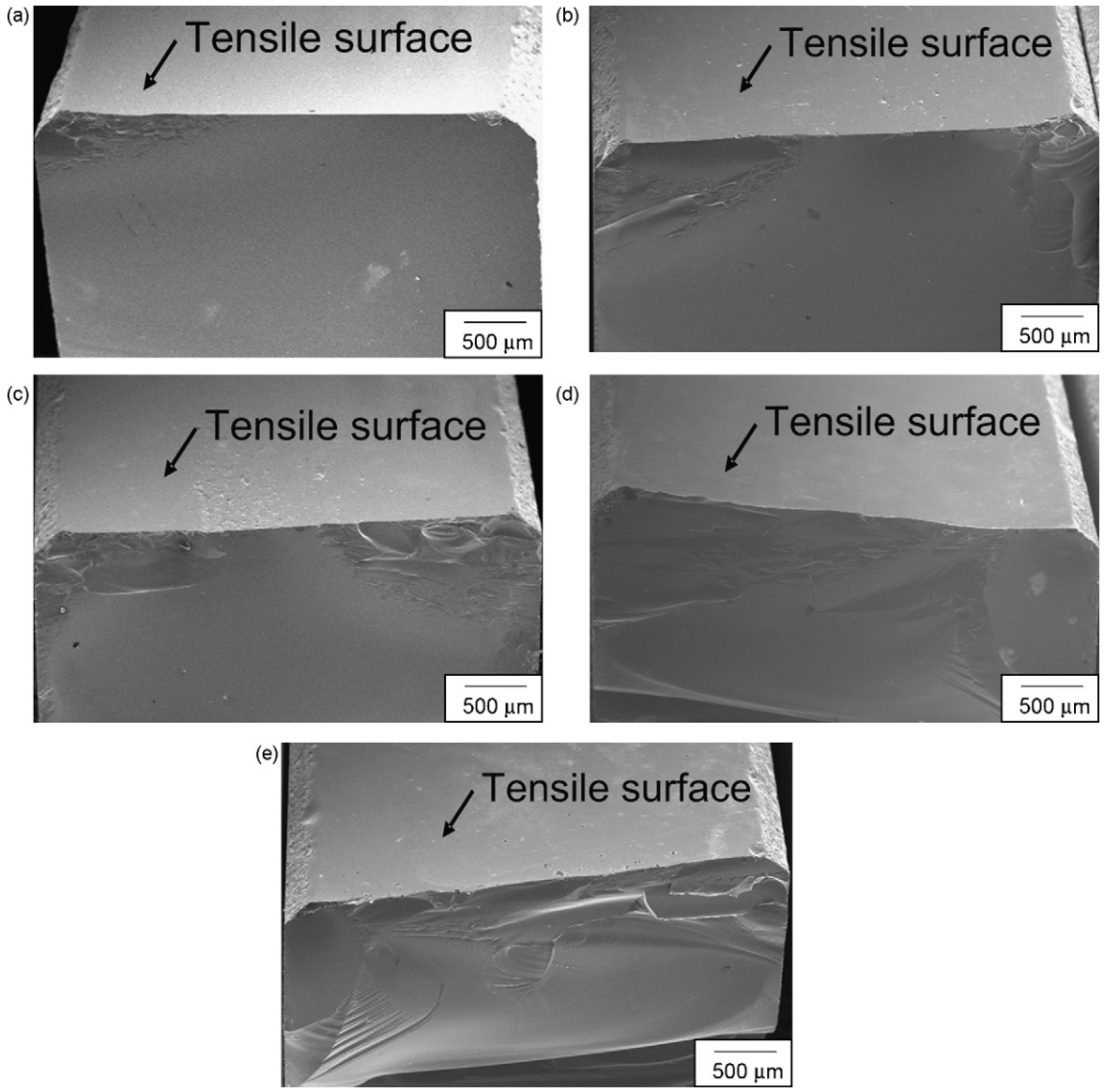

Fig. 7. Typical fracture surfaces of GC-9 specimens tested at (a) 25 °C, (b) 550 °C, (c) 600 °C, (d) 600 °C, and (e) 650 °C.

surfaces showed different morphologies among the given testing temperatures and they could be divided into two fracture patterns. One exhibited a smooth fracture surface and the other showed a rough fracture surface. The specimens fractured at room temperature, 550 °C, and 600 °C (Fig. 7(a–c)) had smoother fracture surfaces with a smaller rough area, but the specimens broken at 600 °C and 650 °C (Fig. 7(d and e)) had larger rough areas. A GC-9 specimen with a greater flexural strength accompanied with a rougher fracture surface due to a higher fracture energy and a less severe surface flaw population. As mentioned above, propagation of a preexisting flaw becomes more difficult at high temperatures because energy dissipation through viscoelastic and/or plastic flow takes place in the vicinity of the flaw [39]. Hence, a larger rough area was observed on the fracture surface of the GC-9 glass tested at 600 °C and 650 °C.

There are two types of fracture surface morphology exhibited at 600 °C. One (Fig. 7(c)) had a smaller rough area like that at room temperature or 550 °C (Fig. 7(a and b)), the other (Fig. 7(d)) had a greater rough zone similar to that at 650 °C (Fig. 7(e)). This might explain why the flexural strength data at 600 °C were more scattering than those at 550 °C and 650 °C and had a smaller value of Weibull modulus.

3.4. Effect of displacement rate at high temperature

As shown in Fig. 3, the GC-9 specimens did not break under a displacement rate of 0.005 mm s^{-1} at 700 °C and 750 °C due to a lower viscosity. The GC-9 glass is expected to be used at a temperature range between 700 °C and 750 °C, so characteristics of the viscous behavior in such a glass sealant at this temperature range need to be further investigated. It is generally known that the viscous behavior of a glass material at high temperature is dependent on the loading or deformation rate. An additional set of four-point bending tests at 750 °C were thus conducted by increasing the displacement rate from 0.005 to 0.05 mm s^{-1}. Fig. 8 shows the force–displacement curves at 750 °C under two displacement rates, 0.005 and 0.05 mm s^{-1}. It is shown in Fig. 8 that the specimen still could not be fractured at 750 °C even though the displacement rate was increased by an order to a value of 0.05 mm s^{-1}. Similar to that of a force–displacement curve for a displacement rate of 0.005 mm s^{-1} at 700 °C (Fig. 3), the force–displacement curve for a displacement rate of 0.05 mm s^{-1} at 750 °C (Fig. 8) shows no continuous increase in force when applying a constant deformation rate on the specimen. Instead, once the force reached a maximum

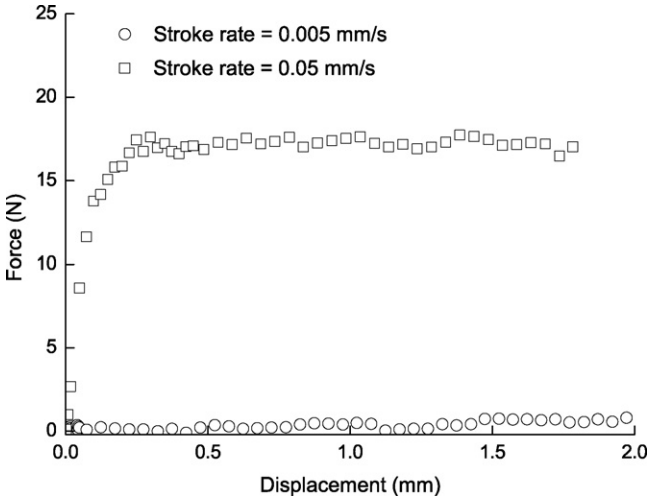

Fig. 8. Typical force–displacement relationship for the GC-9 glass at 750 °C under two different displacement rates.

value, it almost remained constant at this level until the four-point bending test was terminated. However, this maximum force level was increased from 2.5 to 19 N when the displacement rate was increased from 0.005 to 0.05 mm s^{-1} at 750 °C. Apparently, the stress relaxation effect became less effective when the deformation rate was increased by an order of magnitude. The corresponding Young's modulus can be estimated from the linear portion of the force–displacement curve. In this way, the Young's modulus of the GC-9 glass sealant at 750 °C under a displacement rate of 0.05 mm s^{-1} was determined as 22 GPa. Such a value is even greater than the average Young's modulus value (17 GPa) at 700 °C under a displacement rate of 0.005 mm s^{-1}. Apparently, the stiffness or the slope of the linear portion of the load–displacement curve is dependent on strain rate and the Young's modulus of the given glass at a temperature above T_g and T_s can be determined by the four-point bending technique under an appropriate deformation rate.

4. Conclusions

The glass transition temperature (T_g, 668 °C) and the softening temperature (T_s, 745 °C) of the GC-9 glass are the two important temperature indices for mechanical properties. At a temperature below T_g, the flexural strength of the GC-9 was increased with temperature, but its Young's modulus did not significantly change with temperature. When placed at a temperature close to or above T_s, both the flexural strength and Young's modulus of the GC-9 glass were significantly reduced.

Weibull distribution of the flexural strength of the GC-9 glass at various temperatures was obtained. For a given failure probability, the flexural strength of the given glass material was increased from room temperature to 650 °C, presumably, due to a crack healing effect. Such a crack healing effect was also responsible for the variation of Weibull modulus with temperature below T_g.

At 750 °C, which is higher than the softening temperature (745 °C), fracture of the GC-9 specimens did not take place even though the displacement rate was increased from 0.005 to 0.05 mm s^{-1}. This was caused by an in situ stress relaxation effect taking place during the four-point bending test.

Acknowledgement

This work was supported by the National Science Council (Taiwan) under Contract No. NSC 95-2221-E-008-004-MY3.

References

[1] K. Eichler, G. Solow, P. Otschik, W. Schaffrath, J. Eur. Ceram. Soc. 19 (1999) 1101–1104.
[2] K.L. Ley, M. Krumpelt, R. Kumar, J.H. Meiser, I. Bloom, J. Mater. Res. 11 (1996) 1489–1493.
[3] C. Lara, M.J. Pascual, A. Durán, J. Non-Cryst. Solids 348 (2004) 149–155.
[4] K.D. Meinhardt, D.-S. Kim, Y.-S. Chou, K.S. Weil, J. Power Sources 182 (2008) 188–196.
[5] P.A. Lessing, J. Mater. Sci. 42 (2007) 3465–3476.
[6] J.W. Fergus, J. Power Sources 147 (2005) 46–57.
[7] P.H. Larsen, P.F. James, J. Mater. Sci. 33 (1998) 2499–2507.
[8] P.H. Larsen, F.W. Poulsen, R.W. Berg, J. Non-Cryst. Solids 244 (1999) 16–24.
[9] N. Lahl, K. Singh, L. Singheiser, K. Hilpert, J. Mater. Sci. 35 (2000) 3089–3096.
[10] S.-B. Sohn, S.-Y. Choi, J. Non-Cryst. Solids 282 (2001) 221–227.
[11] S.-B. Sohn, S.-Y. Choi, G.-H. Kim, H.-S. Song, G.-D. Kim, J. Non-Cryst. Solids 297 (2002) 103–112.
[12] R. Zheng, S.R. Wang, H.W. Nie, T.-L. Wen, J. Power Sources 128 (2004) 165–172.
[13] S.-B. Sohn, S.-Y. Choi, J. Am. Ceram. Soc. 87 (2004) 254–260.
[14] S.R. Choi, N.P. Bansal, Ceram. Eng. Sci. Proc. 26 (2005) 275–283.
[15] B.N. Nguyen, B.J. Koeppel, S. Ahzi, M.A. Khaleel, P. Singh, J. Am. Ceram. Soc. 89 (2006) 1358–1368.
[16] M.J. Pascual, A. Guillet, A. Durán, J. Power Sources 169 (2007) 40–46.
[17] K.A. Nielsen, M. Solvang, S.B.L. Nielsen, A.R. Dinesen, D. Beeaff, P.H. Larsen, J. Eur. Ceram. Soc. 27 (2007) 1817–1822.
[18] Y.-S. Chou, J.W. Stevenson, R.N. Gow, J. Power Sources 168 (2007) 426–433.
[19] Y.-S. Chou, J.W. Stevenson, R.N. Gow, J. Power Sources 170 (2007) 395–400.
[20] F. Smeacetto, M. Salvo, M. Ferraris, J. Cho, A.R. Boccaccini, J. Eur. Ceram. Soc. 28 (2008) 61–68.
[21] V.A.C. Haanappel, V. Shemet, I.C. Vinke, W.J. Quadakkers, J. Power Sources 141 (2005) 102–107.
[22] C.S. Montross, H. Yokokawa, M. Dokiya, Br. Ceram. Trans. 101 (2002) 85–93.
[23] C.-K. Lin, T.-T. Chen, Y.-P. Chyou, L.-K. Chiang, J. Power Sources 164 (2007) 238–251.
[24] H. Yakabe, Y. Baba, T. Sakurai, M. Satoh, I. Hirosawa, Y. Yoda, J. Power Sources 131 (2004) 278–284.
[25] V.A.C. Haanappel, V. Shemet, S.M. Gross, Th. Koppitz, N.H. Menzler, M. Zahid, W.J. Quadakkers, J. Power Sources 150 (2005) 86–100.
[26] Y.-S. Chou, J.W. Stevenson, P. Singh, J. Power Sources 152 (2005) 168–174.
[27] P. Batfalsky, V.A.C. Haanappel, J. Malzbender, N.H. Menzler, V. Shemet, I.C. Vinke, R.W. Steinbrech, J. Power Sources 155 (2006) 128–137.
[28] Z. Yang, K.D. Meinhardt, J.W. Stevenson, J. Electrochem. Soc. 150 (2003) A1095–A1101.
[29] Z. Yang, G. Xia, K.D. Meinhardt, K.S. Weil, J.W. Stevenson, J. Mater. Eng. Perform. 13 (2004) 327–334.
[30] Y.-S. Chou, J.W. Stevenson, J. Hardy, P. Singh, J. Power Sources 157 (2006) 260–270.
[31] S.R. Choi, N.P. Bansal, A. Garg, Mater. Sci. Eng. A 460–461 (2007) 509–515.
[32] W. Liu, X. Sun, M.A. Khaleel, J. Power Sources 185 (2008) 1193–1200.
[33] C.-K. Liu, T.-Y. Yung, K.-F. Lin, Proceedings of the Annual Conference of the Chinese Ceramic Society 2007 (CD-ROM), 2007 (In Chinese).
[34] C.-K. Liu, T.-Y. Yung, S.-H. Wu, K.-F. Lin, Proceedings of the MRS_Taiwan Annual Meeting 2007 (CD-ROM), 2007 (In Chinese).
[35] C.-K. Liu, T.-Y. Yung, K.-F. Lin, Proceedings of the Annual Conference of the Chinese Ceramic Society 2008 (CD-ROM), 2008 (In Chinese).
[36] ASTM Standard C1211, Standard Test Method for Flexural Strength of Advanced Ceramics at Elevated Temperature, Annual Book of ASTM Standards, vol.15.01, ASTM International, West Conshohocken, PA, USA, 2005, pp. 268–284.
[37] D.W. Richerson, Modern Ceramic Engineering, 2nd ed., Marcel Dekker, Inc., New York, USA, 1992.
[38] R.C. Hibbeler, Statics and Mechanics of Materials, SI ed., Prentice Hall, Inc., Singapore, 2004.
[39] T. Rouxel, J.-C. Sangleboeuf, J. Non-Cryst. Solids 271 (2000) 224–235.
[40] P. Hrma, W.T. Han, A.R. Cooper, J. Non-Cryst. Solids 102 (1988) 88–94.
[41] R.N. Singh, Int. J. Appl. Ceram. Technol. 4 (2007) 134–144.
[42] K.O. Kese, Z.C. Li, B. Bergman, J. Eur. Ceram. Soc. 26 (2006) 1013–1022.
[43] M. Ono, W. Nakao, K. Takahashi, K. Ando, Fatigue Fract. Eng. Mater. Struct. 30 (2007) 1–9.
[44] D.C. Cassidy, N.A. Gjostein, J. Am. Ceram. Soc. 53 (1969) 161–168.